

# NUMERICAL STABILITY STUDY OF MULTI-CIRCLE ELLIPTIC HALO ORBIT IN THE ELLIPTIC RESTRICTED THREE-BODY PROBLEM

Hao PENG<sup>(1)</sup>, and Shijie XU<sup>(2)</sup>

<sup>(1)(2)</sup>*School of Astronautics, Beihang University, Beijing, China, AstroH.Peng@gmail.com*

**Abstract:** *The Multi-circle Elliptic Halo (ME-Halo) orbit is a kind of symmetric resonant period orbit only existing in Elliptic Restricted Three-Body Problem (ERTBP). Its remarkable features includes that it accepts the primary eccentricity  $e$ , has a long period and its stability property bifurcates. The author utilizes continuation methods together with optimization solvers to generate thousands of ME-Halo orbits, and then systematically investigated their stability property variation with parameters  $e$  and mass ratio  $\mu$ . Parameters show complex impacts on the stability. The orbit of some group can possess more than one eigenvalues greater than one. Continuation barriers are observed to be accompanied by a sudden change of the stability. The result in this paper is a pioneering research of periodic orbits with potential practical applications in ERTBP, and it helps understand the dynamic of ERTBP as well.*

**Keyword:** *ERTBP, periodic orbit, stability, ME-Halo, time periodic Poincare section.*

## 1. Introduction

The Circular Restricted Three-Body Problem (CRTBP) has drawn much attentions and fruitful applications in space exploration have been yielded. Since the motion of planets in the solar system can be better described by Kepler's elliptic orbits with eccentricity  $e$  ranging from 0.0086 to 0.2488 [1], research priorities were turned to extending results under CRTBP to the Elliptic Restricted Three-Body Problem (ERTBP) model. The natural choice is to focus on the existence and stability of libration periodic orbits in ERTBP. Broucke had first systematically studied the stability of periodic orbits in planar ERTBP [2]. Three important properties of planar ERTBP is stated as: the absence of Jacobi integral; discrete periodic orbits and two system parameters the mass ratio  $\mu$  and the eccentricity  $e$ . But the study was limited to the planar situation and period orbits were mostly constructed in systems with  $\mu > 0.2$ , which makes them less meaningful in solar system. Sarris continued a vertical Lyapunov orbit with period  $2\pi$  in CRTBP to ERTBP along both  $\mu$  and  $e$ , then he studied their stability and divided the stability coefficients space into 12 regions [3]. But the system he investigated is also with large  $\mu$  which can lead to larger period. His one important state is that the ERTBP model cannot have both axial and bilateral symmetry at the same time. Heppenheimer studied the out-of-plane motion in ERTBP utilizing Jacobi elliptic functions. He constructed linear solution of the out-of-plane motion and used Lindstedt-Poincare method to obtain a third order expansion [4]. He claimed that the eccentricity tended to decrease the period while the nonlinearity tended to increase the period. Recently Hou and Liu constructed analytical expansion of collinear libration point orbits in ERTBP by Lindstedt-Poincare method [5]. The result is really lengthy and complex since the appearance of eccentricity requires the expansion with one more parameter. Gurfil and Kasdin applied niching genetic algorithm to search practically stable geocentric orbits in ERTBP and discussed their applications [6]. These orbits remain finite motion for a long time but they revolve around the primary rather than libration points. Gurfil and Meltzer worked out an analytical approximation of the monodromy matrix of orbits in linearized ERTBP [7], which is helpful in station-keep problem but the study of the

stability requests full model monodromy matrix.

Practical applications of ERTBP are also drawing great attentions, so periodic orbits with interesting properties different from CRTBP orbits are needed to be revealed and investigated, which is partially done in this paper. Hiday and Howell had studied the optimal transfer between libration point orbits in ERTBP since 1992 [8]. Multiple shooting method could also be used to construct Lissajous orbits in ERTBP [9, 10]. Using the same method Mahajan and Pernicka recently investigated the construction of halo like orbits in asteroid ERTBP and proposed their applications [11]. But the stability is studied by one non-periodic circle of the orbit which actually only reflects local stability properties. Campagnola designed the gravitational capture of BepiColombo mission and found that the resulted trajectory shadowed the manifold of a halo like orbit in the Sun-Mercury ERTBP. He calculated elliptic halo orbit possessing commensurable period with primaries and found the stability bifurcation [12]. As an extension of the WSB theory, Hyeraci and Topputo numerically investigated the role of true anomaly in ballistic capture, and proposed a method to help design missions in planar ERTBP [13, 14]. Recently Qi and Xu et al. had studied the ballistic capture in Sun-Mercury ERTBP [15].

In this paper, the systematic study of the stability of Multi-Circle Elliptic Halo (ME-Halo) orbits in ERTBP is presented. First the construction of ME-Halo orbits are elaborated, where continuation and optimization method are used. ME-Halo orbits are continued along both  $\mu$  and  $e$ . Second the method to study their stability is given in detail where the monodromy matrix of ME-Halo orbits is derived. Then the stability result of different ME-Halo orbit groups including the Earth-Moon and the Sun-Mercury system are summarized and analyzed. Interesting features of ME-Halo orbit can provide novel nominal orbit and the understanding of their unique stability properties can help in future space mission design. The result demonstrated here can serve as a fresh supplement to the comprehensive understanding of the ERTBP.

## 2. Dynamic Models

The full three-body problem has no complete solution because there are 18 first order differential equations but only 10 general integrals. An intuitive approach is to study the restricted three-body problem (RTBP), where the mass of one body tends to zero and does not affect primaries' motion. In RTBP the motion of the infinitesimal third body under the attraction of two primaries' gravity fields is of interests. In this section a brief review of equations of motion for the spacecraft in CRTBP and ERTBP is given. In CRTBP primaries revolves each other on Keplerian circular orbit. Nechvile first employed a transform from the inertial coordinate frame to a synodic coordinate frame, with which the equations of motion is concise and there comes the Jacobi integral. As illustrated in Figure 1, the origin locates at the barycenter and the synodic rotating coordinate frame takes  $x$ -axis pointing from the larger primary  $m_1$  to the smaller one  $m_2$ , where  $m_1$  locates at  $x_1 = -\mu$  and  $m_2$  locates at  $x_2 = 1 - \mu$ . The  $z$ -axis is parallel with the primary angular momentum and the  $y$ -axis finishes the right-handed system. The eccentricity  $e$  of the primary orbit (dashed ellipse) is zero in CRTBP. Then the system is scaled by adopting distance between primaries  $r_{12}$  as length unit, the total primary mass  $(m_1 + m_2)$  as weight unit, and the reciprocal of angular velocity  $n$  as time unit. The scaled mass ratio of the smaller primary  $\mu = m_2 / (m_1 + m_2)$  is an important system parameter. In this way, equations of motion for CRTBP is given by [16]

$$\begin{aligned}
\ddot{x} - 2\dot{y} &= \Omega_x \\
\ddot{y} + 2\dot{x} &= \Omega_y \\
\ddot{z} &= \Omega_z
\end{aligned} \tag{1}$$

where

$$\Omega(x, y, z) = \frac{1}{2}(x^2 + y^2) + \frac{1-\mu}{r_1} + \frac{\mu}{r_2} + \frac{1}{2}\mu(1-\mu) \tag{2}$$

with  $r_1 = \sqrt{(x+\mu)^2 + y^2 + z^2}$  and  $r_2 = \sqrt{(x-1+\mu)^2 + y^2 + z^2}$ .

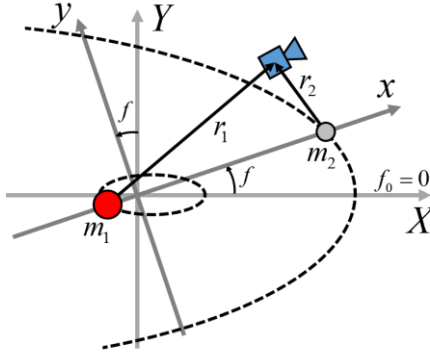


**Figure 1. Barycenter Inertial coordinate frame  $(X, Y, Z)$  and Barycenter Synodic coordinate frame  $(x, y, z)$ . The  $z$ -axis finishes the right handed system point out of the paper. In CRTBP the primary orbit (dashed arc) is circular orbit and in ERTBP it is elliptical.**

In ERTBP primaries rotate each other on a Keplerian elliptic orbit (dashed ellipse in Figure 1). The distance between primaries  $r_{12}$  is changing with true anomaly  $f$ , thus with time  $t$ , and is given as

$$r_{12}(f) = \frac{a_{12}(1-e^2)}{1+e \cos f}$$

where  $a_{12}$  is the semimajor axis of primaries. The synodic coordinate frame is still utilized but is pulsating now. The system is instantaneously scaled by  $r_{12}(f)$ , the total primary mass  $(m_1 + m_2)$  and the reciprocal of the mean angular velocity  $\bar{n}$ . So the synodic frame is not only pulsating but also non-uniformly rotating. Furthermore, the independent variable is transformed from time  $t$  to true anomaly  $f$  by the chain rule

$$\frac{d}{dt} = \frac{df}{dt} \frac{d}{df}$$

Where

$$\frac{df}{dt} = \frac{G(m_1 + m_2)^{1/2}}{a^{3/2}(1-e^2)^{3/2}}(1 + e \cos f)^2 \quad (3)$$

In this way equations of motion of the infinitesimal body in ERTBP is given by [16]

$$\begin{aligned} x'' - 2y' &= \omega_x \\ y'' + 2x' &= \omega_y \\ z'' &= \omega_z \end{aligned} \quad (4)$$

where

$$\omega(x, y, z, f) = (1 + e \cos f)^{-1} \tilde{\Omega}(x, y, z) \quad (5)$$

$$\tilde{\Omega}(x, y, z) = \Omega(x, y, z) - \frac{1}{2} e \cos f z^2 \quad (6)$$

Primes over  $x$ ,  $y$  and  $z$  indicate the differential respect to true anomaly  $f$ . The same coordinate symbol will not cause confusion in the paper. The epoch when primaries are at their periapsis is set to be  $f_0 = 0$  as illustrated in Figure 1. Eq. (1) and (4) shows identical form but in fact  $\omega$  differs from  $\Omega$  greatly as shown by Eq. (6). It is worth noting that ERTBP implicitly depends on time  $t$  through Eq. (3). And because of the trigonometric introduced by Eq. (3), (5) and (6), ERTBP is a non-autonomous system with period  $2\pi$ . Multiplied Eq. (4) by  $\dot{x}$ ,  $\dot{y}$  and  $\dot{z}$  respectively, add them up and integrate, we have

$$\dot{x}^2 + \dot{y}^2 + \dot{z}^2 = 2 \int (\omega_x dx + \omega_y dy + \omega_z dz) \quad (7)$$

Since  $\omega$  depends also on the true anomaly  $f$ , the expression under the integral is not a total differential. Instead we have

$$d\omega = (\omega_x dx + \omega_y dy + \omega_z dz) + \omega_f df$$

Substitute it into Eq. (7) and we have

$$\dot{x}^2 + \dot{y}^2 + \dot{z}^2 = 2\omega - 2 \int_{f_0}^f \omega_f d\tau - C(f_0)$$

The term  $2\omega$  is the amended potential of the third body in synodic frame. The integral term is caused by the pulsating of the system. The integral constant  $C(f_0)$  depends on the initial anomaly  $f$  now. So there is no Jacobi constant in ERTBP anymore. When  $e = 0$  the integral term

vanishes and  $C(f_0)$  degenerates to the traditional Jacobi integral  $C$  in CRTBP.

### 3. ERTBP Periodic Orbits and the Stability

The periodic orbit is the only type of orbits that we can ever hope to understand completely throughout their evolution from the distant past to the distant future since the entire course of their evolution is determined by knowledge over a finite time interval, i.e. the period [17]. Fix point can be viewed as a periodic orbit with zero or infinite period. The mostly investigated periodic orbits in CRTBP include planar and vertical Lyapunov orbit families, prograde and retrograde orbit families around small primary, halo orbit families at  $L_{1,2}$  and horseshoe-shape orbits around  $L_{3,4}$ . But in ERTBP most of these orbits do not survive the perturbation of the eccentricity  $e$  because the libration point is also osculating with primaries now. Therefore a special kind of periodic resonant orbits in ERTBP is introduced in this section.

#### 3.1. ERTBP Libration Point Region

Following the way similar with Euler and Lagrange utilized in CRTBP, libration points in ERTBP can be obtained. Letting the first and second order differential terms in Eq. (4) equal to zero, we have

$$\omega_x = \omega_y = \omega_z = 0 \quad (8)$$

The solution gives five libration points in the synodic frame which locates exactly at the same position as CRTBP in synodic coordinate frame. However they are only geometrically ones but not dynamical ones or equilibriums anymore, because the frame is pulsating thus collinear points are oscillating along the  $x$ -axis and triangular points are oscillating to maintain the central configuration with primaries [18]. In spite of this, the libration point region is still bounded, thus orbits can still revolve around the region.

#### 3.2. ME-Halo Orbits

Despite libration points, generally periodic solutions in ERTBP are not easy to detect. The ERTBP is non-autonomous but periodic and it keeps the invariance under the map [3]

$$X(f; x, y, z, \dot{x}, \dot{y}, \dot{z}) \rightarrow X(-f; x, -y, z, -\dot{x}, \dot{y}, -\dot{z}) \quad (9)$$

which indicates symmetric with respect to  $x$ - $z$  plane. In CRTBP the Lyapunov orbit family and the halo orbit family satisfy the map. According to the symmetry with respect to  $x$ - $z$  plane, Moulton in 1920 expressed [19] and Broucke in 1969 [2] cited the strong periodicity criterion for planar ERTBP as following,

*For an orbit to be periodic it is sufficient that it has two perpendicular crossings with the syzygy-axis, and that the crossings happen at moments when the two primaries are at an apse, (i.e., at maximum or minimum elongation, or apoapsis and periapsis).*

Campagnola expanded it to spatial problem and obtained a similar sufficient criterion [12],

*For an orbit to be periodic in the ERTBP, it is sufficient that it has two perpendicular crossing*

with either the normal plane or the syzygy axis, or both of them, when the primaries are at apse.

It is clear that because of the periodicity of the system, symmetric periodic orbits in ERTBP can only take period  $T_E$  commensurable with the system period  $2\pi$

$$T_E = 2K\pi, K \in \mathbb{R}^+ \quad (10)$$

Compared with Lissajous orbits and quasi-halo orbits, halo orbits have precise period and are relatively easy to calculate. So halo orbits are chosen as study objects and are continued into ERTBP. At the beginning a proper orbit period  $T_E$  should be chosen. The period range of the halo orbit family with small  $\mu$  in CRTBP is too narrow to possess integer multiples of primary period  $2\pi$ . Therefore halo orbits revolving  $M$  circles while primaries revolving  $N$  circles are concerned and thus we have

$$T_E = M \cdot T_C = 2N\pi / M, M, N \in \mathbb{N}^+$$

This condition is referred to as *commensurable constrain* hereinafter. Since there is no available analytical method that can provide halo orbits with precise period  $T_C$ , the orbit is extracted from the whole halo orbit family numerically. First the period curve of the whole orbit family is generated to find out and choose a proper set of  $(M, N)$ . Second the initial condition of the corresponding orbit is obtained by dichotomy. For example, in Figure 2 the period curve of Earth-Moon  $L_1$  and  $L_2$  halo orbit families are depicted. The vertical lines correspond to proper  $(M, N)$ s. There are infinite sets of  $(M, N)$ s although they distribute discretely. It is worth note that  $M$  grows faster than  $N$ , which will cause numerical difficulties as discussed later.

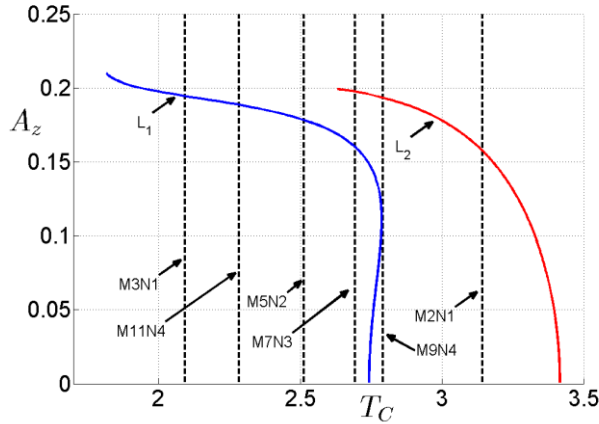


**Figure 2. The period curve of circular halo orbit families in Earth-Moon CRTBP model.**

After having got  $T_E$  for  $e = 0$ , increase the eccentricity  $e$  by step  $\delta e$ , use the previously obtained periodic orbit as initial guess, then adjust initial condition to close up the periodic orbit by multi-segment optimization method as discussed in section 4.1. In this way a group of orbits parameterized by  $e$  can be obtained. In similarly way a group of orbits parameterized by the mass

ratio  $\mu$  can be obtained. Obtained orbits in Earth-Moon system are demonstrated in Figure 3 and Figure 4.

These periodic orbits stay around the libration point region for such a long time, which is  $N$  times of the primary period. Since the emphases is paid on their multi-circle property in this paper, they are referred to as *Multi-circle Elliptic Halo (ME-Halo)* orbits hereinafter, and halo orbits in CRTBP are referred to as *circular halo orbits* for clarity. Campagnola had once constructed some ME-Halo orbits in Earth-Moon system and referred to them as Elliptic Halo Orbits [12].

### 3.3. Four ME-Halo Orbit Groups

In CRTBP the halo orbit family exists continuously, but in ERTBP ME-Halo orbits are discrete because of the commensurable constrain. However they can be continuously parameterized by  $\mu$  and  $e$ . For clarity the term *orbit group* rather than *orbit family* in CRTBP is used in the following discussion.

According to the periodicity criterion, ME-Halo orbits perpendicularly cross the  $x$ - $z$  plane twice and the two crosses can occur whether primaries are at periapsis or apoapsis. If  $M$  is odd, two crosses occur at two sides of ME-Halo and the orbit is different whether it starts at  $f_0 = 0$  or  $f_0 = \pi$ . Define *Periapsis Group* to start from either side at  $f_0 = 0$  and *Apoapsis Group* to start at  $f_0 = \pi$ . In Figure 3 the Earth-Moon  $L_2$  periapsis group and apoapsis group ME-Halos with  $M5N2$  are depicted. The most obvious difference between them is that the position where the perpendicular cross occurs, as marked by red small circle. For periapsis ME-Halo it occurs at the outer circle while for apoapsis at the inner circle as shown in  $y$ - $z$  projection.

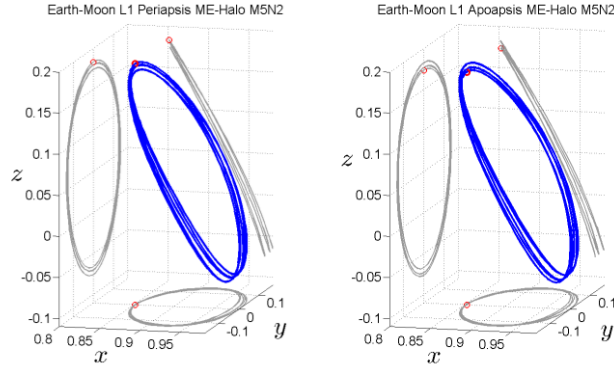


**Figure 3. Earth-Moon  $L_2$  Periapsis (left plot) and Apoapsis (right plot) ME-Halo orbit with  $M5N2$ .**

If  $M$  is even, two crosses occur at the same side of ME-Halo and the orbit can be different whether the cross is on the left or right side as shown on the  $x$ - $y$  projection in Figure 4. Define *Left Group* to start from the left side at  $f_0 = 0$  and *Right Group* from the right side. The Earth-Moon  $L_2$  left group and right group ME-Halo orbits with  $M2N1$  are depicted. The most obvious difference is whether the position where the orbit bifurcate is at the top or the bottom. Besides, we have north and south circular halo orbits in CRTBP, therefore each group here possesses a north and a south

branch as well. In this paper the north branch is chosen as the study object.

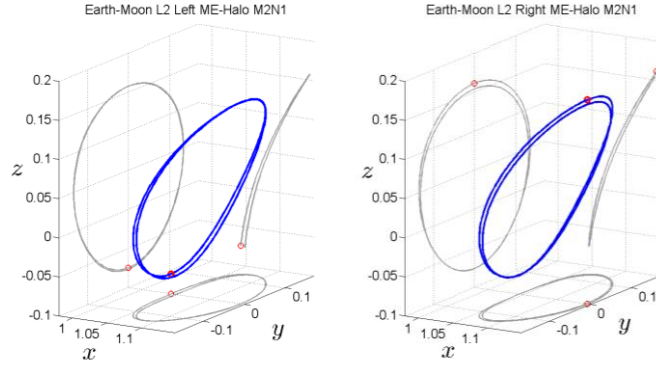


**Figure 4. Earth-Moon  $L_2$  Left (left plot) and Right (right plot) ME-Halo orbit with  $M2N1$ .**

### 3.4. Stability of ME-Halo and Stable Indices

Given a periodic non-autonomous system

$$\dot{x} = g(x, t), \quad g(x, t+T) = g(x, t), \quad x \in \mathbb{R}^n \quad (11)$$

In order to determine the stability of a periodic solution  $\bar{x}(t, t_0)$ , its nearby solutions should be considered. Assume  $\bar{x}(t, t_0)$  is perturbed to  $x(t, t_0)$  by  $\delta x(t, t_0)$  as

$$x(t, t_0) = \bar{x}(t, t_0) + \delta x(t, t_0)$$

Substitute it into Eq. (11), expand at  $\bar{x}$  and we have

$$\dot{\bar{x}} + \delta \dot{x} = g(\bar{x} + \delta x, t) = g(\bar{x}, t) + Dg(\bar{x}, t)\delta x + O(|\delta x|^2)$$

Using the fact that  $\dot{\bar{x}} = g(\bar{x}, t)$ , it becomes

$$\delta \dot{x} = Dg(\bar{x}, t)\delta x + O(|\delta x|^2)$$

For stability questions, we are concerned with the behavior the solutions arbitrarily close to  $\bar{x}(t, t_0)$ , so it is reasonable that we focus on the associated linearized system [17]

$$\delta \dot{x} = Dg(\bar{x}, t)\delta x \quad (12)$$

This is a linear periodic non-autonomous system. Applying Fluquet theory, Its state transition matrix  $\Phi(t, t_0)$  consists of  $n$  linearly independent solutions and satisfies

$$\dot{\Phi}(t, t_0) = \text{Dg}(\bar{x}, t)\Phi(t, t_0), \quad \Phi(t_0, t_0) = I_n \quad (13)$$

The monodromy matrix of  $\bar{x}(t, t_0)$  is defined as the transition matrix over one period  $\Psi(t_0) = \Phi(t_0 + T, t_0)$ . The periodic orbit is stable if and only if all eigenvalues of  $\Psi(t_0)$  have modules smaller than one. Because eigenvalues of  $\Psi(t_0)$  is invariant along the periodic orbit [20], it can be simply referred to as  $\Psi$  without specifying the epoch at which it is evaluated.

The stability of ME-Halo orbits is investigated through its monodromy matrix  $\Psi$ . In CRTBP eigenvalues of the monodromy matrix of the circular halo orbit are a pair of unit eigenvalues, a pair of reciprocal real eigenvalues and a pair of reciprocal complex eigenvalues on unit circle [21]. But in ERTBP there are no unit eigenvalues anymore because of the appearance of eccentricity  $e$  [2]. The eigenvalues of ME-Halo orbits in ERTBP come in reciprocal pairs as

$$\lambda_1, 1/\lambda_1, \lambda_2, 1/\lambda_2, \lambda_3, 1/\lambda_3$$

Following the notation of Broucke and Sarris, the stability index of ME-Halo is defined as

$$k_i = \lambda_i + 1/\lambda_i, \quad i = 1, 2, 3$$

This gives a simple criterion that the orbit is unstable if  $k_i \leq 2$ . The only exception is that two pairs of reciprocal complex eigenvalues is conjugated but not on the unit circle, where they give complex  $k_{2,3}$  but the orbit is still unstable. So the definition is modified to be

$$k_j = 2 \max(\|\lambda_j\|, \|1/\lambda_j\|) \text{ if } \|\lambda_j\| \neq 1, \quad j = 2, 3. \quad (14)$$

The reciprocal complex eigenvalues will give  $k_j > 2$  because at least one of them is out of the unit circle. In this way, the criterion is sufficient and necessary. Obviously this definition will cause discontinuity in the index curve as a function of  $\mu$  or  $e$ , but the discontinuity is helpful to detect sudden change of the stability which does not exists in CRTBP.

## 4. Numerical Method

In this section, the numerical method used to continue circular halo into ME-Halo and to integrate the monodromy matrix over such a long period are elaborated in detail.

### 4.1. Multi-Segment Optimization in ERTBP

The description of correcting a ME-Halo orbit as an optimization problem is presented in this section. Define the state vector of ERTBP as  $X(f) = [x, y, z, \dot{x}, \dot{y}, \dot{z}]^T$ . The initial state  $X(f_0)$  of the ME-Halo orbit and half period state  $X(f_0 + T_E/2)$  obtained by integrating Eq. (4) are

$$X_0 = X(f_0) = [x_0, 0, z_0, 0, \dot{y}_0, 0]^T$$

$$X_{T_1} = X(f_0 + T_E / 2) = [x_1, y_1, z_1, \dot{x}_1, \dot{y}_1, \dot{z}_1]^T$$

where  $T_1 = T_E / 2 = N\pi$  is the half period. According to the periodicity criteria of ERTBP,  $X_{T_1}$  should be perpendicular to the  $x$ - $z$  plane, i.e.  $\hat{y}_1 = \hat{x}_1 = \hat{z}_1 = 0$ . Hence the cost function is defined as

$$\min J(X_0) = \sqrt{(\hat{y}_1 - y_1)^2 + (\hat{x}_1 - \dot{x}_1)^2 + (\hat{z}_1 - \dot{z}_1)^2}$$

Where the hat over symbols indicate the target zero state. The differential constrains is given by Eq. (4). It is worthy to note that the independent variable is true anomaly  $f$  in ERTBP now.

Even utilize optimization method, the algorithm costs too long time when  $M$  is large or the step  $\delta e$  or  $\delta \mu$  is large. In this case, we borrow the idea of the multiple shooting method introduced by Howell and Pernicka for calculating Lissajous orbits in CRTBP [10]. The orbit is broken into  $n$  segments and constrained to be continuous and smooth as illustrated in Figure 5. Similar to the description above, the multi-segment optimization problem is described below as,

$$\begin{aligned} \min J(X_0, f_0; \dots; X_i, f_i; \dots; X_{n-1}, f_{n-1}) \\ = \sqrt{(\hat{y}_{T_1} - y_{T_1})^2 + (\hat{x}_{T_1} - \dot{x}_{T_1})^2 + (\hat{z}_{T_1} - \dot{z}_{T_1})^2} \end{aligned}$$

with the same differential constrains given by Eq. (4) and linear constrains as

$$X_i = X_i^-, \quad i=1, \dots, n-1$$

where  $X_i$  and  $f_i$  is the starting state and epoch of the  $(i+1)$ -th segment,  $X_i^-$  is the integration end of the  $i$ -th segment starting from  $X_{i-1}$ .

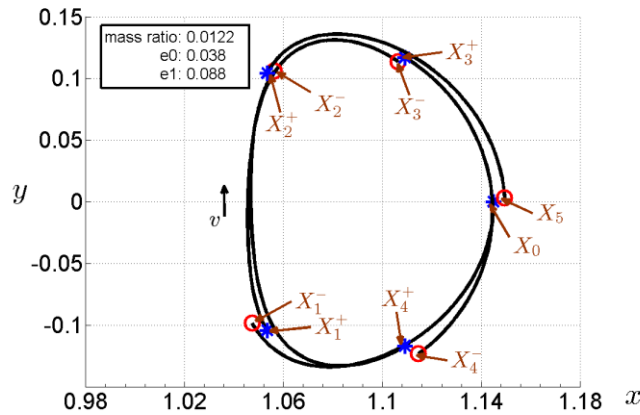


**Figure 5. Multi-segments optimization illustration.**

The convergence of the algorithm increases as  $n$  increases, but the time cost increases as well. So

after a trial and error process, we choose  $M/2 \leq n \leq 2M$  for  $e$  continuation and  $n \geq 3M$  for  $\mu$  continuation. Compared with multiple shooting method, the optimization problem is easier to handle, program and extend. In this way ME-Halo orbits can be constructed relatively easily and more focus can be paid on their special stability properties.

## 4.2. Monodromy Matrix

In ERTBP, the monodromy matrix is calculated by numerically integrate the state transition matrix  $\Phi$  for a whole period  $T_E$ . Substitute equations of motion of ERTBP, i.e. Eq. (4), into Eq. (13) and we have

$$\dot{\Phi}(f, f_0) = A_E(X, f)\Phi(f, f_0), \quad \Phi(f_0, f_0) = I_6 \quad (15)$$

where  $A_E(X, f) = Dg(X, f)$  is the Jacobian of the Eq. (4)

$$A_E(X, f) = \begin{bmatrix} 0 & I_3 \\ H_E & K_E \end{bmatrix}_{(X, f)}, \quad H_E = \begin{bmatrix} \omega_{xx} & \omega_{xy} & \omega_{xz} \\ \omega_{yx} & \omega_{yy} & \omega_{yz} \\ \omega_{zx} & \omega_{zy} & \omega_{zz} \end{bmatrix}_{(X, f)}, \quad K_E = \begin{bmatrix} 0 & 2 & 0 \\ -2 & 0 & 0 \\ 0 & 0 & 0 \end{bmatrix}$$

The monodromy matrix  $\Psi_E$  of ME-Halo is then obtained by propagating Eq. (4) together with Eq. (15) from  $f_0$  to  $f_0 + T_E$ . For Periapsis, Left and Right Group ME-Halo orbits  $f_0 = 0$  is adopted and for Apoapsis Group  $f_0 = \pi$  is adopted. When the ME-Halo orbit is given by multi-segment optimization method, there will be always tiny state errors at the connection points. If we integrate  $\Psi_E$  directly from the first starting point for one period, these errors will be accumulated and exaggerated greatly. Notice that the Monodromy matrix is essentially a linear differential matrix equation, hence we have

$$\begin{aligned} \Psi_E &= \Phi(f_0 + T_E, f_0) = I_6 \cdot \exp\left(\int_{f_0}^{f_0 + T_E} A_E(X, \tau) d\tau\right) \\ &= I_6 \cdot \exp\left(\int_{f_{n-1}}^{f_0 + T_E} A_E d\tau\right) \cdot I_6 \cdot \exp\left(\int_{f_{n-2}}^{f_{n-1}} A_E d\tau\right) \cdots I_6 \cdot \exp\left(\int_{f_0}^{f_1} A_E d\tau\right) \\ &= \Phi(f_0 + T_E, f_{n-1}) \cdots \Phi(f_2, f_1) \cdot \Phi(f_1, f_0) \end{aligned}$$

Therefore  $\Psi_E$  can be calculated along each segment simultaneously and then multiplied up. In this way the exaggeration of errors can be suppressed.

## 5. Results and Discussions

In this paper the stability of different  $L_1$  and  $L_2$  ME-Halo orbits with various parameters  $\mu$  and  $e$  is studied. The parameter region analyzed here is spanned by  $\mu \in [0.001, 0.020]$  and  $e \in [0, 0.210]$  with constant step sizes  $\delta\mu = 0.001$  and  $\delta e = 0.001$ . In this region many choices

of  $(M,N)$  for each  $\mu$  are available,  $L_1$  Periapsis and Apoapsis ME-Halo orbits with  $M5N2$  are chosen as study objects here. The ME-Halo orbit in the Earth-Moon system and the Sun-Mercury system are also investigated. During the computation orbits are firstly continued along  $\mu$  and then continued along  $e$ . Totally thousands of orbits are obtained by parallel computing and are organized in separated database. Then the eigenvalue database of monodromy matrix are calculated. The stability of orbits is analyzed by the stability indices of their monodromy matrixes and presented at the last. Computational precisions and other important parameters adopted during the calculation are listed in Tab. 1.

**Table 1. Computational precision and other important parameters adopted in this paper**

Name	Value
Integration tolerance	$3 \times 10^{-14}$
Differential correction tolerance	$1 \times 10^{-9}$
Optimization tolerance	$1 \times 10^{-9}$
Optimization stop tolerance	$1 \times 10^{-7}$
Monodromy differential stepsize	$1 \times 10^{-8}$
Earth-Moon mass ratio $\mu$	0.0122
Earth-Moon eccentricity $e$	0.0554
Sun-Mercury mass ratio $\mu$	$1.66 \times 10^{-7}$
Sun-Mercury eccentricity $e$	0.2056

During the study, the mass ratio  $\mu$  is observed to have a greater impact than eccentricity  $e$  on ME-Halo orbits. The ME-Halo orbit is needed to break into more than 32 segments to accomplish one step continuation by  $\delta\mu$ , but only 8 to 12 segments for  $\delta e$ . This can be explained by the fact that in the Legendre polynomial expansion of Eq. (4)  $\mu$  arises from the first-order term but  $e$  appears only from the second-order term. Unexpected, ME-Halo orbits cannot be continued to arbitrary eccentricity  $e$  in small mass ratio  $\mu_{\max} < \hat{\mu}$ . A closer look at their stability indices curve reveals that the stability changes before the failure of continuation. This also occurs in the Sun-Mercury system, but luckily the Earth-Moon system is found to be just above the separatrix. Other significant properties and details are elaborated in the following discussion.

### 5.1. Stability Bifurcation

Campagnola once observed that the stability of left and right ME-Halo orbits in the Earth-Moon system bifurcates at  $e=0$  [12]. More bifurcations and collisions of the eigenvalues of the monodromy matrix are observed. In Figure 6, all eigenvalue configuration types encountered during the study are depicted. In the center the circular halo orbit with  $e=0$  is presented. In Type 3 there is a pair of negative real eigenvalues and two pair of real ones. In Type 4 there are two pairs of reciprocal eigenvalues locating neither on the unit circle or the real axis. In all types except 3 the largest real eigenvalues persists and other two pairs of eigenvalues distribute differently. Only one or some Types appear for one certain group of ME-Halo orbits and they transform through bifurcation and collision. It is noteworthy that Type 3, 5 and 6 have two or three pairs of real eigenvalues associated with each point on ME-Halo orbits, which happens in real planet system as discussed in section 5.4.

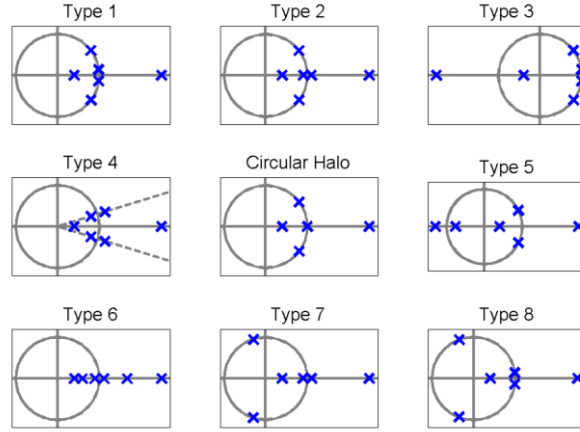


**Figure 6. Distribution types of eigenvalues of monodromy matrix of ME-Halo orbits obtained during the study in this paper. The plot in the center is the schematic of eigenvalues of circular halo orbit.**

## 5.2. Periapsis Group ME-Halo

In this section the stability of  $L_1$  periapsis group ME-Halo orbits with  $M5N2$  is investigated. The evolution of stable indices  $k_i$  with respect to  $\mu$  and  $e$  is plotted separately in Figure 7, Figure 8 and Figure 9. The Earth-Moon system parameter is represented by the dot (red) on the surface (the same in following figures). As revealed by the stability indices surfaces, the orbit is generally greatly unstable and the instability increases with  $\mu$  for fixed  $e$ . There is a great gap observed around  $\hat{\mu} \approx 0.012$  in all figures. The trend of the surface on two sides is different. When  $\mu < \hat{\mu}$  the instability decreases with  $e$  and when  $\mu > \hat{\mu}$  the instability increases with  $e$ . Also the continuation along  $e$  stops earlier than expected when  $\mu < \hat{\mu}$  but success for all  $e$  when  $\mu > \hat{\mu}$ , as most clearly shown in Figure 7.

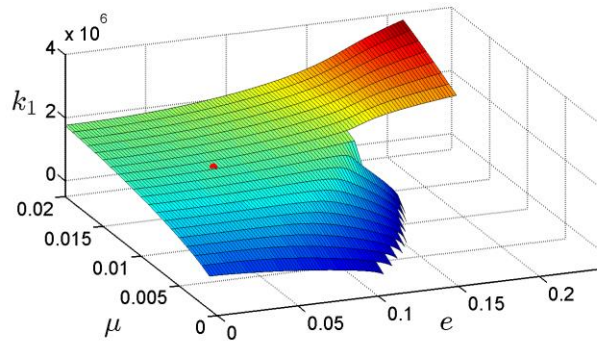


**Figure 7.  $k_1$  with respect to both  $\mu$  and  $e$  ( $L_1$  Periapsis Group ME-Halo with  $M5N2$ ). The Earth-Moon system parameter is represented by the dot (red) on the surface.**

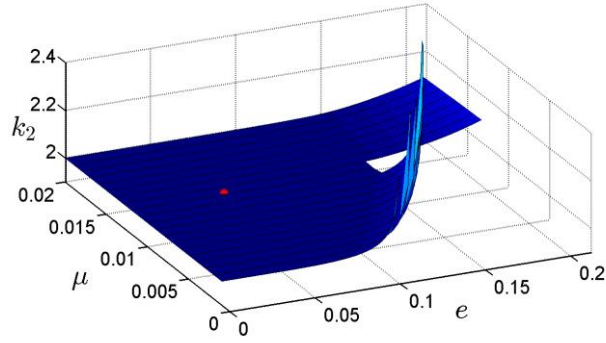


**Figure 8.**  $k_2$  with respect to both  $\mu$  and  $e$  (L1 Periapsis Group ME-Halo with  $M5N2$ )

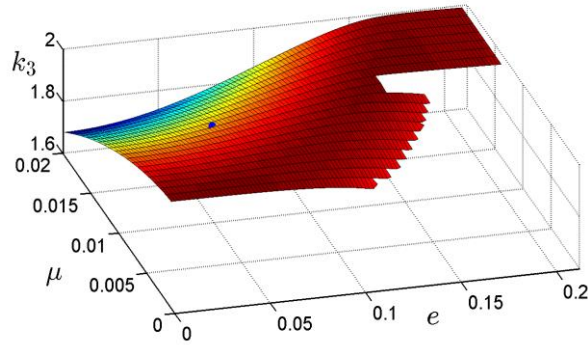


**Figure 9.**  $k_3$  with respect to both  $\mu$  and  $e$  (L1 Periapsis Group ME-Halo with  $M5N2$ ).

Since the existence of the  $\hat{\mu}$  stops the continuation somehow, a detailed study and closer look of the effect of  $\mu$  on the curve  $k_i(e)$  is presented in figures below. In Figure 10, there is a clear gap around the curve for  $\hat{\mu}=0.012$ . The curve keeps increasing when  $\mu > \hat{\mu}$  but decreases and stopped soon when  $\mu < \hat{\mu}$ . In the zoon-in plot, the curve falls down to below zero, which means the  $k_1$  enters the linearly stable region in a certain range of  $\mu$  and  $e$ . The end of the curve is nearly vertical and there seems to be infinite discontinuities point, which explains the failure of the continuation process. In Figure 11, when  $\mu < \hat{\mu}$   $k_2$  grows bigger than 2 and then suddenly falls down to the stable region, but when  $\mu > \hat{\mu}$   $k_2$  increases steadily and smoothly. In the zoon-in plot the different tendency is more clear. In Figure 12,  $k_3$  keeps smaller than 2, and the zoon-in plot reveals that the  $k_3$  curve for  $\mu = \hat{\mu}$  reaches 2 and stopped. Judging from three indices curves, the bifurcation path of this ME-Halo group along with  $e$  is: for  $\mu < \hat{\mu}$ : Type 2  $\rightarrow$  Stable  $\rightarrow$  Type 3  $\rightarrow$  Stop; for  $\mu > \hat{\mu}$ : Type 2. Moreover, a more delicate study is needed to reveal what happens around  $\hat{\mu} \approx 0.012$ .

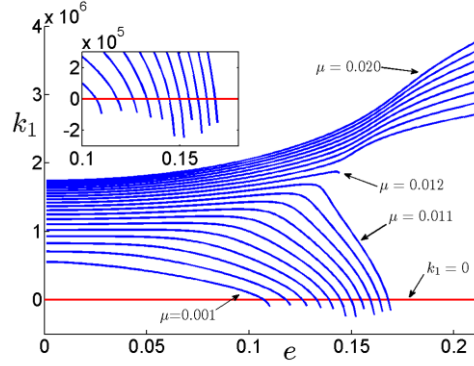


Figure 10. Stable index curve  $k_1(e)$  (L1 Periapsis Group ME-Halo with M5N2)

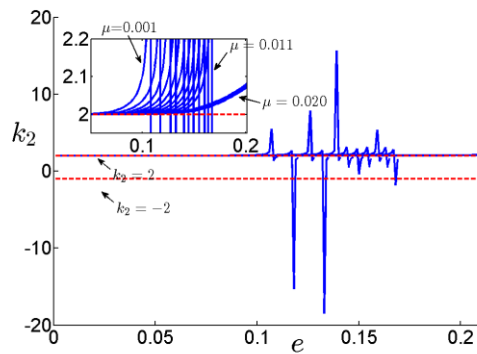


Figure 11. Stable index curve  $k_2(e)$  (L1 Periapsis Group ME-Halo with M5N2)

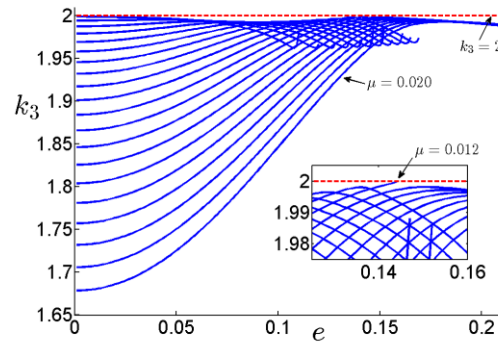
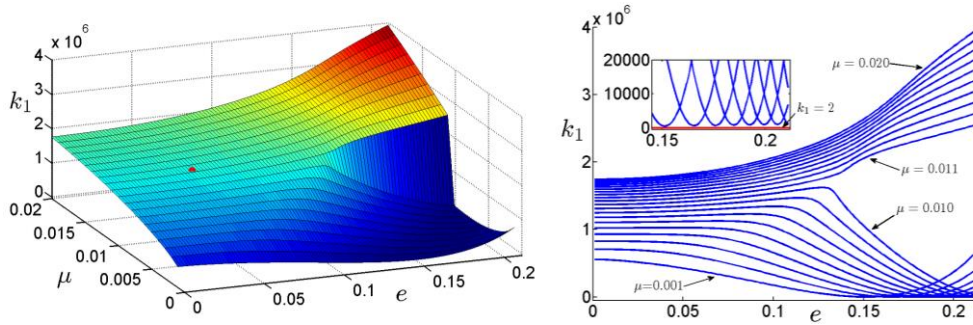


Figure 12. Stable index curve  $k_3(e)$  (L1 Periapsis Group ME-Halo with M5N2)

### 5.3. Apoapsis Group ME-Halo

In this section the stability of  $L_1$  apoapsis group ME-Halo orbits with M5N2 is investigated. Similarly surfaces and curves of  $k_i$  are depicted in figures below. In Figure 13, the surface of  $k_1(e, \mu)$  is smooth but the tendency of the surface has a gap at  $\hat{\mu}$ ,  $0.010 < \hat{\mu} < 0.011$ . In the curve plot at left  $k_1$  is found staying above the stable region though when  $\mu < \hat{\mu}$  it falls down to as small as 500. This is a significant difference from previous Periapsis Group, and it guarantees

the successful continuation to  $e=0.210$ . In Figure 14  $k_2$  (darker blue) and  $k_3$  (lighter green) are plotted together. The different tendency before and after  $\hat{\mu}$  still exists and the clear discontinuity here is caused by the definition of  $k_2$  and  $k_3$  in Eq. (14), which indicates there is a Type 4 configuration. These two indices curves coincide at middle part of curves, which corresponds to that eigenvalues collision at Type 1 and bifurcate to Type 4. Later they bifurcate again, which corresponds to that eigenvalues collision again, at unit circle when  $\mu < \hat{\mu}$  and at real axis when  $\mu > \hat{\mu}$ . Judging from these indices curves, the bifurcation path of this ME-Halo group along with  $e$  is: for  $\mu < \hat{\mu}$ : Type 1  $\rightarrow$  Type 4  $\rightarrow$  Type 1  $\rightarrow$  Type 8  $\rightarrow$  Type 5  $\rightarrow$  Type 8  $\rightarrow$  Type 1; for  $\mu > \hat{\mu}$ : Type 1  $\rightarrow$  Type 4  $\rightarrow$  Type 6. The evolution of eigenvalues is complexity. For some specific parameters there can be more than one pair of real eigenvalues.



**Figure 13. Surface and curves of  $k_1$  with respect to both  $\mu$  and  $e$  (L1 Apoapsis Group ME-Halo with  $M5N2$ )**

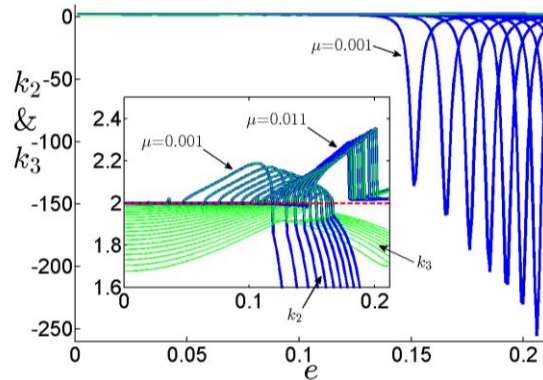


**Figure 14.  $k_2$  (darker blue) and  $k_3$  (lighter green) with respect to both  $\mu$  and  $e$  (L1 Apoapsis Group ME-Halo with  $M5N2$ )**

## 5.4. ME-Halos in Planet System

### 5.4.1. Earth-Moon System

The period curve of the circular halo orbit family in CRTBP is demonstrated in Figure 2. ME-Halo orbits studied in this paper are demonstrated in Figure 3 and Figure 4. The Earth-Moon system parameter is represented by a small dot on the surface in previous discussions. Four Earth-Moon ME-Halo orbits are all greatly unstable. The  $L_1$  Periapsis ME-Halo orbit with  $M5N2$  has two

pairs of real eigenvalues and one pair of complex unit eigenvalues, which is significantly different from circular halo orbits. The  $L_1$  Apoapsis ME-Halo orbit has one pairs of real eigenvalues and two pairs of complex unit eigenvalues.

### 5.4.2. Sun-Mercury System

The mass ration  $\mu_{S.M.}$  of the Sun-Mercury system is too small to be included in the previous figures. Circular halo orbit families at  $L_{1,2}$  are obtained by continuation and corresponding period curves are depicted in Figure 15. The appropriate period chosen in for ME-Halo orbits are  $M5N2$  and  $M7N3$  as annotated in figures, whose  $N$  are not too big thus shorter integration time.

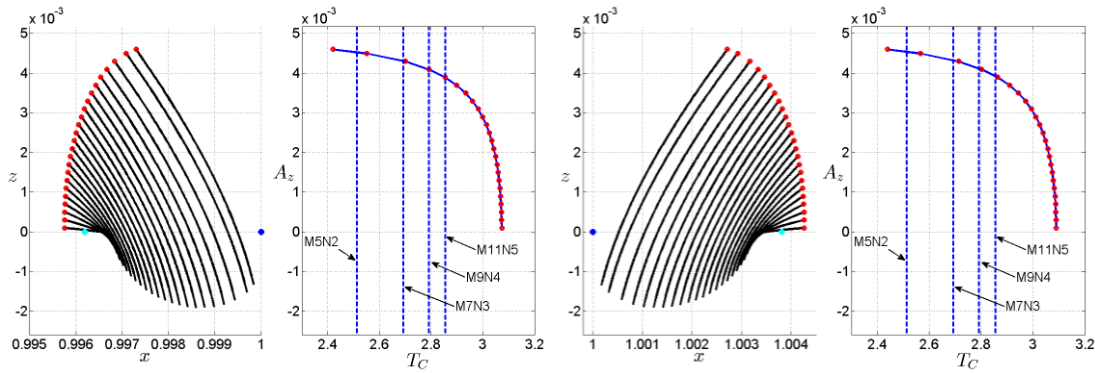


**Figure 15. The  $x$ - $z$  projection view of Sun-Mercury  $L_1$  (left) and  $L_2$  (right) Circular Halo families and their corresponding period curves with respect to  $z$ -axis amplification  $A_z$**

However, in the following process the continuation of ME-Halo orbits with  $M5N2$  stopped at around  $e \approx 0.023$ . According to the tendency of the stability of Periapsis ME-Halo discussed in section 5.2, the barrier occurs much earlier as  $\mu$  is much smaller now. On the other hand, the continuation of ME-Halo orbits with  $M7N3$  successes. The obtained Sun-Mercury  $L_1$  and  $L_2$  Periapsis and Apoapsis ME-Halos are presented in Figure 16 and Figure 17. The difference between them are similar to that of the Earth-Moon system as discussed before. But the stretch of the orbit along all axis directions are greater because the eccentricity is much greater now.

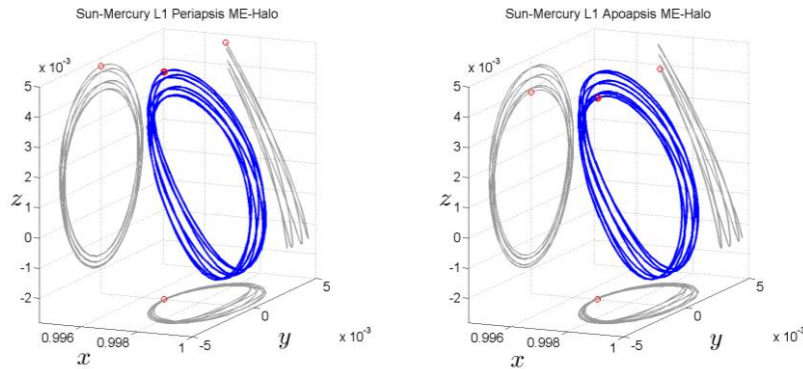


**Figure 16. Sun-Mercury  $L_1$  Periapsis (left) and Apoapsis (right) ME-Halo orbit with  $M7N3$**

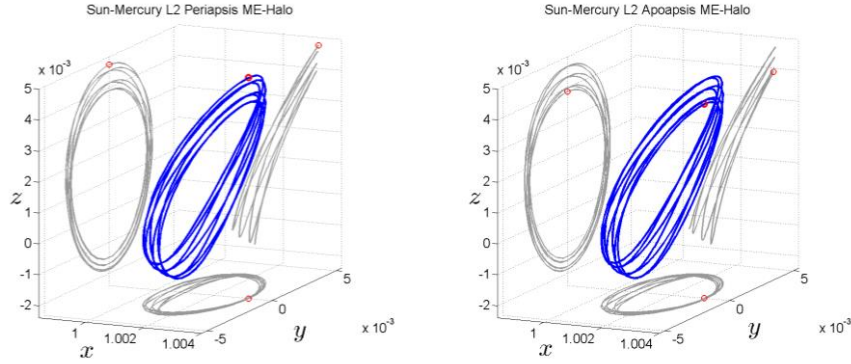


**Figure 17. Sun-Mercury L2 Periapsis (left) and Apoapsis (right) ME-Halo orbit with  $M7N3$**

The accurate propagation of their monodromy matrices is achieved by the multi-segment product. But the extracting of its eigenvalues by simple Matlab command is beyond the machine precision. Because largest eigenvalues obtained is around  $8 \times 10^{10}$ , thus the minimal eigenvalues should be of the order of  $10^{-10}$ . Only the largest eigenvalues is believed to be accurate and it is larger than  $8 \times 10^{10}$  in all groups. Redundant pairs of real eigenvalues of Periapsis ME-Halo orbits are also observed but not accurate enough.

As a summary the ME-Halo orbit is generally unstable, and its stability variation with system parameters is of great complexity. In this paper only one example of each group is studied, thus the result obtained should not be extended to the whole group rashly. But because the symmetry of ERTBP with respect to  $x$ - $y$  plane, results should be correct to corresponding south ME-Halo orbits as well. Moreover, the method utilized in this paper is demonstrated to be effective and it can be easily extended to other situations.

## 6. Conclusion

In this paper the author constructed ME-Halo orbits and systematically studied their stability. The orbit is generated by continuing circular halo orbits to ERTBP model using mature optimization solver. Using this method  $L_1$  Periapsis and Apoapsis Group of ME-Halo orbits are constructed in the region  $\mu \in [0.001, 0.020]$  and  $e \in [0, 0.21]$ . The variation of the stability with the system parameters  $\mu$  and  $e$  are demonstrated and analyzed by stability indices. During the stability investigation different eigenvalue configuration types are observed. Many ME-Halo orbits have more than one pair of real eigenvalues, which is significantly different from circular halo orbits in CRTBP. There are continuation barriers encountered for periapsis ME-Halo orbits. At the end the result of Earth-Moon and Sun-Mercury system is summarized. The interesting stability features of ME-Halo orbits can provide practical applications. The long period  $T_E = M \cdot T_C = 2N\pi$  of ME-Halo orbits indicates longer station-keeping maneuver intervals thus fewer fuel cost, which can provide a better nominal orbit for observation missions like JWST and TPF. Its multi-circle and time-dependent property permits settling  $N$  satellite on a ME-Halo at any given epoch to construct a nature formation fly with priori determined distances. And periapsis and apoapsis can be utilized together to get a  $2N$  nature formation in ERTBP. Moreover, it is easier to choose an optimal orbit from discrete  $(M, N)$ s.

## 7. References

- [1] Russell, R. P., "Survey of Spacecraft Trajectory Design in Strongly Perturbed Environments," *Journal of Guidance, Control, and Dynamics*, Vol. 35, No. 3, pp. 705–720, 2012.
- [2] Broucke, R. A., "Stability of periodic orbits in the elliptic, restricted three-body problem," *AIAA Journal*, Vol. 7, No. 6, pp. 1003–1009, 1969.
- [3] Sarris, E., "Families of symmetric-periodic orbits in the elliptic three-dimensional restricted three-body problem," *Astrophysics and Space Science*, Vol. 162, No. 1, pp. 107–122, 1989.
- [4] Heppenheimer, T. A., "Out-of-plane motion about libration points: Nonlinearity and eccentricity effects," *Celestial Mechanics*, Vol. 7, No. 2, pp. 177–194, 1973.
- [5] Hou, X. Y. and Liu, L., "On motions around the collinear libration points in the elliptic restricted three-body problem," *Monthly Notices of the Royal Astronomical Society*, Vol. 415, No. 4, pp. 3552–3560, 2011.
- [6] Gurfil, P. and Kasdin, N. J., "Niching genetic algorithms-based characterization of geocentric orbits in the 3D elliptic restricted three-body problem," *Computer Methods in Applied Mechanics and Engineering*, Vol. 191, No. 49-50, pp. 5683–5706, 2002.
- [7] Gurfil, P. and Meltzer, D., "Semi-Analytical Method for Calculating the Elliptic Restricted Three-Body Problem Monodromy Matrix," *Journal of Guidance, Control, and Dynamics*, Vol. 30, No. 1, pp. 266–271, 2007.
- [8] Hiday, L. A. and Howell, K. C., "Transfers between libration-point orbits in the elliptic restricted problem," *Celestial Mechanics and Dynamical Astronomy*, Vol. 58, No. 4, pp. 317–337, 1994.
- [9] Pernicka, H. J., "The numerical determination of nominal libration point trajectories and development of a station-keeping strategy," *Purdue Univ*, 1990.
- [10] Howell, K. C. and Pernicka, H. J., "Numerical determination of Lissajous trajectories in the restricted three-body problem," *Celestial Mechanics and Dynamical Astronomy*, Vol. 41, pp. 107–124, 1987.
- [11] Mahajan, B. and Pernicka, H. J., "Halo Orbits Near Small Bodies in the Elliptic Restricted Problem," *AIAA/AAS Astrodynamics Specialist Conference*, Reston, Virginia, pp.1–9, 2012.
- [12] Campagnola, S., "New techniques in astrodynamics for moon systems exploration," *University Of Southern California*, 2010.

- [13] Hyeraci, N. and Topputo, F., “The role of true anomaly in ballistic capture,” *Celestial Mechanics and Dynamical Astronomy*, 2013.
- [14] Hyeraci, N. and Topputo, F., “Method to Design Ballistic Capture in the Elliptic Restricted Three-Body Problem,” *Journal of Guidance, Control, and Dynamics*, Vol. 33, No. 6, pp. 1814–1823, 2010.
- [15] Qi, Y., Xu, S. and Qi, R., “Study of the gravitational capture at mercury in the elliptic restricted three-body problem,” *Proceedings 24th International Symposium on Space Flight Dynamics – 24th ISSFD*, 2014.
- [16] Szebehely, V. G., *Theory of Orbits - The Restricted Problem of Three Bodies*, Academic Press, New York and London, 1967.
- [17] Wiggins, S., *Introduction to applied nonlinear dynamical systems and chaos*, J.E. Marsden, L. Sirovich and S.S. Antman, 2003.
- [18] Meyer, K. R., Hall, G. R. and Offin, D., *Introduction to Hamiltonian Dynamical Systems and the N-Body Problem*, Springer New York, New York, NY, 2009.
- [19] Moulton, F. R., *Periodic Orbits*, Washington Carnegie Institution of Washington, Washington, 1920.
- [20] Bittanti, S. and Colaneri, P., *Periodic Systems*, Springer London, London, 2009.
- [21] Parker, J. S. and Anderson, R. L., *Low-Energy Lunar Trajectory Design*, 2013.